Numerical evaluation of the nonlinear Gribov-Levin-Ryskin-Mueller-Qiu evolution equations for nuclear parton distribution functions

J. Rausch,[1,2] V. Guzey,[3,4] and M. Klasen[2,5]

[1]*Humboldt University Berlin, Department of Physics, Newtonstraße 15, 12489 Berlin, Germany*
[2]*Institut für Theoretische Physik, Westfälische Wilhelms-Universität Münster, Wilhelm-Klemm-Straße 9, 48149 Münster, Germany*
[3]*University of Jyvaskyla, Department of Physics, P.O. Box 35, FI-40014 Jyvaskyla, Finland*
[4]*University of Helsinki, Helsinki Institute of Physics, P.O. Box 64, FI-00014 Helsinki, Finland*
[5]*School of Physics, The University of New South Wales, Sydney, New South Wales 2052, Australia*

(Received 5 December 2022; accepted 20 February 2023; published 2 March 2023)

We numerically study for the first time the nonlinear GLR-MQ evolution equations for nuclear parton distribution function (nPDFs) to next-to-leading order accuracy and quantify the impact of gluon recombination at small x. Using the nCTEQ15 nPDFs as input, we confirm the importance of the nonlinear corrections for small $x \lesssim 10^{-3}$, whose magnitude increases with a decrease of x and an increase of the atomic number A. We find that at $x = 10^{-5}$ and for heavy nuclei, after the upward evolution from $Q_0 = 2$ GeV to $Q = 10$ GeV, the quark singlet $\Omega(x, Q^2)$ and the gluon $G(x, Q^2)$ distributions become reduced by 9%–15%, respectively. The relative effect is much stronger for the downward evolution from $Q_0 = 10$ GeV to $Q = 2$ GeV, where we find that $\Omega(x, Q^2)$ is suppressed by 40%, while $G(x, Q^2)$ is enhanced by 140%. These trends propagate into the $F_2^A(x, Q^2)$ nuclear structure function and the $F_L^A(x, Q^2)$ longitudinal structure function, which after the downward evolution become reduced by 45% and enhanced by 80%, respectively. Our analysis indicates that the nonlinear effects are most pronounced in $F_L^A(x, Q^2)$ and are already quite sizable at $x \sim 10^{-3}$ for heavy nuclei. We have checked that our conclusions very weakly depend on the choice of input nPDFs. In particular, using the EPPS21 nPDFs as input, we obtain quantitatively similar results.

DOI: 10.1103/PhysRevD.107.054003

I. INTRODUCTION

In quantum chromodynamics (QCD), the microscopic structure of hadrons (pions, protons, nuclei) is described in terms of various quark and gluon (commonly called parton) distribution functions (PDFs). As follows from the QCD collinear factorization theorem [1], the PDFs $f_i(x, Q^2)$ are universal, process-independent distributions, which depend on the parton flavor i, the parton light-cone momentum fraction of the parent hadron x, and the resolution scale Q. While the dependence on x cannot be calculated from first principles, the Q^2 dependence of $f_i(x, Q^2)$ is given by the Dokshitzer-Gribov-Lipatov-Altarelli-Parisi (DGLAP) evolution equations [2–5]. In QCD and in any other quantum field theory with a dimensionless coupling constant, the Q^2 dependence of PDFs originates from renormalization of collinear divergences appearing in the ladder-type Feynman graphs (in the physical axial gauge) describing the emission of quarks and gluons with high transverse momenta (parton splitting) [6]. The resulting renormalization group equations are the DGLAP Q^2 evolution equations, which resum the leading $\alpha_s^k \alpha_s \ln Q^2$ contributions to these ladder graphs, where $k = 0$ (leading-order of perturbation theory), $k = 1$ (next-to-leading order, NLO), etc., and $\alpha_s(Q^2)$ is the QCD running coupling constant.

The standard DGLAP evolution equations have been derived in the limit of large Q^2 and $x \sim 1$ and are linear in the parton distributions. The parton splitting encoded in these equations results in an increase of the quark and, especially, the gluon distributions at small x, when one increases the value of Q^2. When the gluon density becomes sufficiently large at small x, one needs to take into account the effects of gluon recombination (gluon-gluon fusion) leading to nonlinear corrections to the DGLAP evolution equations [7–10]. In the Gribov-Levin-Ryskin-Mueller-Qiu (GLR-MQ) approach [7,8,10], the gluon recombination is addressed by analyzing so-called "fan" diagrams, where two gluon ladders merge into a gluon or a quark-antiquark pair. Adding these contributions to the DGLAP equations

yields the nonlinear GLR-MQ evolution equations [8,11], where the nonlinear term tames the growth of the PDFs at small x and leads to their suppression. This can be viewed as a precursor of the gluon saturation at small x [12].

Effects of small-x nonlinear corrections to the DGLAP evolution equations due to gluon recombination have been extensively studied in the literature [13–21]. It was found that these corrections affect the gluon distribution in the proton at small x, $x \lesssim 10^{-3}$, and the interpretation and description of the Hadron-Electron Ring Accelerator (HERA) data on the total and diffractive electron-proton (ep) deep-inelastic scattering (DIS) cross sections at very small $x \sim 10^{-5}$. The effect of the nonlinear corrections is expected to be larger in heavy nuclei and also in models assuming the presence of gluonic "hot spots" in the proton [22]. This and many other topics of small-x QCD constitute an essential part of the physics programs of future electron-ion colliders including the Electron-Ion Collider (EIC) in the U.S. [23], the Large Hadron-Electron Collider (LHeC) [24,25] and the Future Circular Collider (FCC) [26] at CERN, which will allow one to access ep DIS at as low as $x \sim 10^{-4}$ and $x \sim 10^{-6}$, respectively.

The aim of the present work is to study numerically for the first time the nonlinear corrections in the GLR-MQ evolution equations for nuclear parton distribution functions (nPDFs) to NLO accuracy. To this end, we extend the numerical algorithm realized in the well-tested QCDNUM16 DGLAP evolution code [27] and write a stand-alone GLR-MQ evolution program. As input, we use one of the state of the art nPDFs, namely the nCTEQ15 nPDFs [28], which have been obtained by performing a global QCD fit of the data on lepton-nucleus DIS, Drell-Yan lepton pair production in proton-nucleus scattering at Fermilab, and inclusive pion production in deuteron-gold scattering at Relativistic Heavy Ion Collider (RHIC). We then solve the GLR-MQ equations numerically and quantify the effect of the nonlinear corrections in these equations on the evolved nPDFs and the nuclear structure function $F_2^A(x, Q^2)$ and the longitudinal structure function $F_L^A(x, Q^2)$. We find that, as expected, the nonlinear corrections are important for small $x \lesssim 10^{-3}$ and their magnitude increases with a decrease of x and with an increase of the atomic number A. For the smallest studied value of $x = 10^{-5}$, after the upward evolution from $Q_0 = 2$ GeV to $Q = 10$ GeV, the quark singlet $\Omega(x, Q^2)$ and the gluon $G(x, Q^2)$ distributions in heavy nuclei are suppressed compared to their DGLAP-evolved counterparts by 9%–15%, respectively. The relative effect is much stronger for the downward evolution from $Q_0 = 10$ GeV to $Q = 2$ GeV, where we find that $\Omega(x, Q^2)$ is suppressed by 40% compared to the nCTEQ15 PDFs, while $G(x, Q^2)$ is enhanced by 140%. This trend can be explained by the observation that the gluon-gluon recombination plays a much bigger role than the gluon-quark splitting. The behavior of nPDFs translates into the corresponding behavior of the $F_2^A(x, Q^2)$ and $F_L^A(x, Q^2)$ nuclear structure functions. In particular, after the downward evolution from high to low Q and for heavy nuclei and very small x, we observe that $F_2^A(x, Q^2)$ dominated by $\Omega(x, Q^2)$ is reduced by 45%, while $F_L^A(x, Q^2)$ dominated by $G(x, Q^2)$ is enhanced by 80%. We have also checked that these findings very weakly depend on the choice of input nPDFs and obtained quantitatively similar results using the EPPS21 nPDFs [29] as input.

The remainder of the paper is organized as follows. In Sec. II, we present our algorithm for the numerical solution of the DGLAP and GLR-MQ evolution equations. The results of our numerical evaluation of the GLR-MQ equations for nPDFs and predictions for the $F_2^A(x, Q^2)$ and $F_L^A(x, Q^2)$ nuclear structure functions are given in Sec. III. Finally, we summarize our findings in Sec. IV.

II. NUMERICAL SOLUTION OF GLR-MQ EVOLUTION EQUATIONS

The standard DGLAP evolution equations have the following form for the singlet quark $\Omega(x, Q^2) = x\Sigma(x, Q^2) = x\sum_{i=u,d,s,c,\ldots}(q_i(x, Q^2) + \bar{q}_i(x, Q^2))$ and the gluon $G(x, Q^2) = xg(x, Q^2)$ momentum densities (distributions),

$$\frac{\partial \Omega(x, Q^2)}{\partial \ln Q^2} = \frac{\alpha_s(Q^2)}{2\pi}\int_x^1 \frac{dz}{z^2} x\left[P_{FF}\left(\frac{x}{z}\right)\Omega(z, Q^2) + P_{FG}\left(\frac{x}{z}\right)G(z, Q^2)\right],$$
$$\frac{\partial G(x, Q^2)}{\partial \ln Q^2} = \frac{\alpha_s(Q^2)}{2\pi}\int_x^1 \frac{dz}{z^2} x\left[P_{GF}\left(\frac{x}{z}\right)\Omega(z, Q^2) + P_{GG}\left(\frac{x}{z}\right)G(z, Q^2)\right], \quad (1)$$

where P_{FF}, P_{FG}, P_{GF}, and P_{GG} are the quark-quark, gluon-quark, quark-gluon, and gluon-gluon splitting functions calculated to the desired order in α_s [1,30]. Our numerical analysis in this paper is carried out to NLO accuracy.

As we discussed in the Introduction, the gluon recombination modifies the standard DGLAP equations and leads to the following nonlinear GLR-MQ evolution equations [8,11]

$$\frac{\partial\Omega(x,Q^2)}{\partial\ln Q^2}=\left.\frac{\partial\Omega(x,Q^2)}{\partial\ln Q^2}\right|_{\mathrm{DGLAP}}-\frac{27}{160}\frac{\alpha_s^2(Q^2)}{R^2Q^2}(G(x,Q^2))^2,$$
$$\frac{\partial G(x,Q^2)}{\partial\ln Q^2}=\left.\frac{\partial G(x,Q^2)}{\partial\ln Q^2}\right|_{\mathrm{DGLAP}}-\frac{81}{16}\frac{\alpha_s^2(Q^2)}{R^2Q^2}\int_x^1\frac{dz}{z}(G(z,Q^2))^2, \tag{2}$$

where $\partial\Omega(x,Q^2)/\partial\ln Q^2|_{\mathrm{DGLAP}}$ and $\partial G(x,Q^2)/\partial\ln Q^2|_{\mathrm{DGLAP}}$ refer to the right-hand side of Eq. (1). R is the characteristic radius of the gluon distribution in the hadronic target, which determines the strength of the nonlinear corrections. Note that an additional term containing the higher-dimensional gluon distribution G_{HT}, which is suppressed by one power of $\ln 1/x$ and which does not correspond to the gluon distribution, has been neglected in Eq. (2). Since the nonsinglet combinations of quark PDFs do not mix with the gluon distribution and, hence, do not receive corrections due to gluon recombination, we do not consider them in our analysis.

We numerically solve the GLR-MQ evolution equations using the "brute force" method in the momentum space. To do it, we extend the numerical algorithm used in the QCDNUM16 DGLAP evolution code [27] to take into account the nonlinear corrections in Eq. (2) and implement it in a stand-alone evolution code. QCDNUM16 is a fast QCD evolution program, which numerically evolves PDFs using the DGLAP evolution equations to LO and NLO accuracy in the $\overline{\mathrm{MS}}$ factorization scheme. The program can handle flavor thresholds (light quark variable flavor number scheme or heavy quark fixed flavor number scheme) and allows one to independently vary the renormalization and factorization scales. QCDNUM16 and its more recent variants constitute an important part of the open-source xFitter project [31,32] providing a framework for the determination of the PDFs using QCD fits to the available data with lepton (HERA) and hadron (Tevatron, the Large Hadron Collider) beams.

Below we outline our approach.

Equations (1) and (2) are evaluated numerically on an $x-Q^2$ grid. Given the parton distributions at a starting value Q_0^2, the distributions at other values of Q^2 are determined by solving a set of four equations at each grid point, which are derived using spline interpolation between grid points. The grid consists of $n+1$ values of x bounded by x_0 and 1, $x_0<\ldots<x_n=1$, and $m+1$ values of Q^2, which are all above or below Q_0^2. The values of x and Q^2 are spaced logarithmically because the region of low x and Q^2 is most relevant for our purpose. In the following, $D(x_c,Q_r^2)=D_{rc}$ refers to $\Omega(x,Q^2)$ or $G(x,Q^2)$ evaluated at the grid point (x_c,Q_r^2), and the corresponding logarithmic derivative $\partial D/\partial\ln Q^2$ is written as D'. At $x=1$, $D_{rn}=0$ for all r.

To compute the convolution integrals in Eqs. (1) and (2), D is interpolated linearly between x-values,

$$D_x(x,Q_r^2)=\bar{a}_1x+\bar{a}_0,\quad \text{for } x\in[x_k,x_{k+1}]. \tag{3}$$

By imposing the continuity condition $D_x(x_i,Q_r^2)=D_{ri}$ for $i=k,\,k+1$, one obtains

$$D_x(x,Q_r^2)=(1-t_k)D_{rk}+t_kD_{r(k+1)},$$
$$\text{where } t_k=\frac{x-x_k}{x_{k+1}-x_k}\in[0,1]. \tag{4}$$

With this, the integrals can be written as weighted sums over D_{rk}, where k runs from c to n. Assuming D_{rk} is known for $k>c$ (condition 1), the only unknowns in the DGLAP equations are Ω_{rc}, Ω'_{rc}, G_{rc}, and G'_{rc}. Two more equations relating these unknowns can be obtained by using a quadratic interpolation between Q^2-values,

$$D_Q(x_c,Q^2)=\tilde{a}_2(\ln Q^2)^2+\tilde{a}_1\ln Q^2+\tilde{a}_0,$$
$$\text{for } Q^2\in[Q_{r-1}^2,Q_r^2]. \tag{5}$$

The requirements that $D_Q(x_c,Q_i^2)=D_{ic}$ and $D'_Q(x_c,Q_i^2)=D'_{ic}$ for $i=r-1,r$ imply that

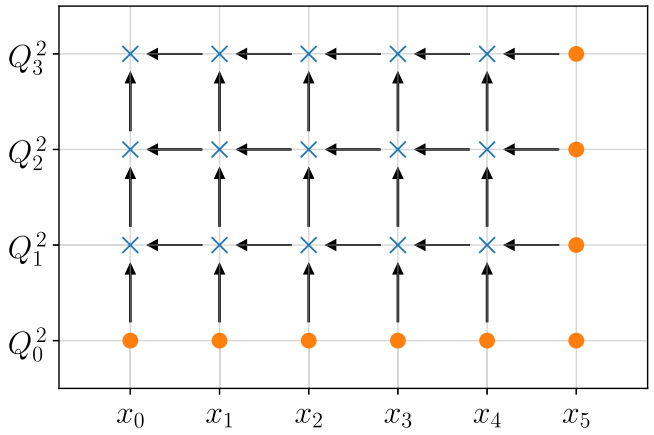

FIG. 1. The evolution path through a grid with $n=5$ and $m=3$. Every row is evaluated from the right to the left, starting at the bottom and going to the top. The orange dots indicate the starting values of D.

$$D_{rc} = D_{(r-1)c} + \frac{\Delta_r}{2}(D'_{(r-1)c} + D'_{rc}), \tag{6}$$

where $\Delta r = \ln Q_r^2 - \ln Q_{r-1}^2$. If $D_{(r-1)c}$ and $D'_{(r-1)c}$ have been calculated during the previous evolution steps (condition 2), Eq. (6) and the DGLAP equations can be solved for the four unknowns.

The path through the grid must now be chosen such that conditions 1 and 2 are satisfied for any grid point (x_c, Q_r^2), where D is being evaluated. This is achieved by starting at $x_n = 1$ for every value of Q^2 and proceeding toward smaller x, as illustrated in Fig. 1.

Using the linear interpolation of Eq. (4), the convolution integrals in the DGLAP equations can be written as

$$\int_{x_c}^1 \frac{dz}{z^2} x_c P_{AB}\left(\frac{x_c}{z}\right) D(z, Q_r^2) = \sum_{k=c}^{n-1} \omega_{AB}(x_k, x_c) D_{rk}, \tag{7}$$

where

$$\omega_{AB}(x_k, x_c) = \begin{cases} S_1(f_{c+1}, f_c) & \text{if } k = c \\ S_1(f_{k+1}, f_k) - S_2(f_k, f_{k-1}) & \text{else} \end{cases} \tag{8}$$

with $f_k = x_c/x_k$ and

$$S_i(u, v) = \frac{a_i}{v-u} \int_u^v \frac{dz}{z}(z - b_i) P_{AB}(z), \tag{9}$$

where $a_1 = b_2 = v$ and $a_2 = b_1 = u$. The weights $w_{AB}(x_k, x_c)$ are calculated numerically at program initialization.

The discretized DGLAP equations can then be expressed in the following form

$$\begin{aligned} \Omega'_{rc} &= W_{FF}\Omega_{rc} + W_{FG} G_{rc} + M_F, \\ G'_{rc} &= W_{GF}\Omega_{rc} + W_{GG} G_{rc} + M_G, \end{aligned} \tag{10}$$

where $W_{AB} = \alpha_s/(2\pi) w_{AB}(x_c, x_c)$ and M_F and M_G contain the summands with $k > c$ multiplied by $\alpha_s/(2\pi)$. Together with Eq. (6), they form a system of four linear equations with four unknowns. This system is solved numerically at every step in the evolution.

The nonlinear correction in the GLR-MQ evolution equations involves the gluon distribution squared, see Eq. (2). The difficulty presents only the second line in Eq. (2), where the nonlinear term is expressed as an integral of $(G(z, Q^2))^2$. To numerically implement it, one uses the linear interpolation in z for $G(z, Q^2)$, see Eqs. (3) and (4), substitutes it in Eq. (2), and obtains the following discretized expression for the nonlinear correction,

$$\int_{x_c}^1 \frac{dz}{z} G^2(z, Q_r^2) = \sum_{k=c}^{n-1} w_1(x_k) G_{rk}^2 + \sum_{k=c}^{n-2} 2 w_2(x_k) G_{r(k+1)} G_{rk}, \tag{11}$$

where

$$\begin{aligned} w_1(x_k) &= \begin{cases} T_1(x_c, x_{c+1}) & \text{if } k = c \\ T_1(x_k, x_{k+1}) + T_2(x_{k_1}, x_k) & \text{else} \end{cases} \\ w_2(x_k) &= -T_3(x_k, x_{k+1}) \end{aligned} \tag{12}$$

and

$$T_i(u, v) = \frac{1}{(v-u)^2} \int_u^v \frac{dz}{z}(c_i d_i - (c_i + d_i) z + z^2), \tag{13}$$

where $c_1 = d_1 = d_3 = v$ and $c_2 = d_2 = c_3 = u$. Note that since the nonlinear correction is expressed in terms of the gluon distribution squared, Eq. (11) contains both the G_{rk}^2 terms and the $G_{r(k+1)} G_{rk}$ cross terms [compare to Eq. (7)].

The computation of $w_1(x_k)$ and $w_2(x_k)$ can be done much faster than that of the DGLAP weights $w_{AB}(x_k, x_c)$: Only $\mathcal{O}(n)$ integrals must be calculated instead of $\mathcal{O}(n^2)$, and the integrand in Eq. (13) is much simpler than the splitting functions in Eq. (7).

With this, the discretized form of the GLR-MQ evolution equations read

$$\begin{aligned} \Omega'_{rc} &= W_{FF}\Omega_{rc} - V_1 G_{rc}^2 + W_{FG} G_{rc} + M_F, \\ G'_{rc} &= W_{GF}\Omega_{rc} - V_2 G_{rc}^2 + (W_{GG} - V_3) G_{rc} + M_G - N_G, \end{aligned} \tag{14}$$

where $V_1 = (27/160) f(Q_r^2)$, $V_2 = (81/16) f(Q_r^2) w_1(x_c)$, $V_3 = (81/16) f(Q_r^2) 2 w_2(x_c) G_{r(c+1)}$, and $f(Q_r^2) = \alpha_s^2(Q_r^2)/(R^2 Q_r^2)$. The N_G term contains the remainder of the sums in Eq. (11) multiplied by the factor of $(81/16) f(Q_r^2)$. Since Eq. (6) still applies, there are again four equations relating D_{rc} and D'_{rc}, which can be solved at each grid point, when using the evolution path shown in Fig. 1.

Using the numerical approach outlined above, we solved the GLR-MQ evolution equations on a 50×40 grid ($n = 50$, $m = 40$) in the x-Q^2 plane using the nCTEQ15 [28] and EPPS21 [29] nPDFs for the initial condition, which have been accessed via the LHAPDF6 framework [33]. This grid size is sufficient to provide a better than 1.2% numerical accuracy for the interpolation in x and Q^2.

For the running strong coupling constant $\alpha_s(Q^2)$, we used the standard NLO expression [1] along with the requirements that $\alpha_s(M_Z^2) = 0.118$, where $M_Z = 91.2$ GeV is the Z boson mass, and that $\alpha_s(Q^2)$ is continuous across the

charm quark mass $m_c = 1.3$ GeV and the bottom quark mass $m_b = 4.5$ GeV flavor thresholds.

For a nuclear target with the mass number A, we take $R = 1.25\ \text{fm} \times A^{1/3}$. Note that since nuclear PDFs scale approximately as A, the nonlinear term in Eq. (2) scales as $A^{4/3}$, which significantly enhances the importance of the nonlinear corrections for heavy nuclei compared to the proton case. However, in practice, the significant nuclear shadowing of the gluon distribution at small x and the rather dilute distribution of nucleons in nuclei reduce the net effect [34].

To test the accuracy of our evolution code, as an example, we used the nCTEQ15 nPDFs for Au-197 as the initial conditions at $Q_0 = 2$ GeV, evolved them up to $Q = 10$ GeV neglecting the nonlinear GLR-MQ correction, and found that the resulting quark singlet and gluon distributions in the $10^{-5} \le x \le 10^{-3}$ interval agree with the nCTEQ15 parametrization with an accuracy of around 1.2%.

III. RESULTS FOR NUCLEAR PDFs AND STRUCTURE FUNCTIONS

In this section, we present results of our numerical studies of the nonlinear GLR-MQ evolution equations for the nCTEQ15 and EPPS21 nPDFs, quantify the effect of the nonlinear corrections in these equations on the evolved nPDFs and the nuclear structure function $F_2^A(x, Q^2)$ and the longitudinal structure function $F_L^A(x, Q^2)$, and thus determine the kinematic regions in the $x - Q^2$ plane, where the nonlinear corrections are potentially important.

Figure 2 presents the results of GLR-MQ evolution for the quark singlet (left panels) and the gluon (right panels) nPDFs divided by A for the heavy nucleus of Au-197 as a function of the momentum fraction x. In the two upper panels, the dashed curves labeled "GLR-MQ" show the results the upward evolution from $Q_0 = 2$ GeV to $Q = 4$ GeV and $Q = 10$ GeV. They are compared to the nCTEQ15 parametrization at the corresponding values of Q given by the solid curves. As expected, the recombination

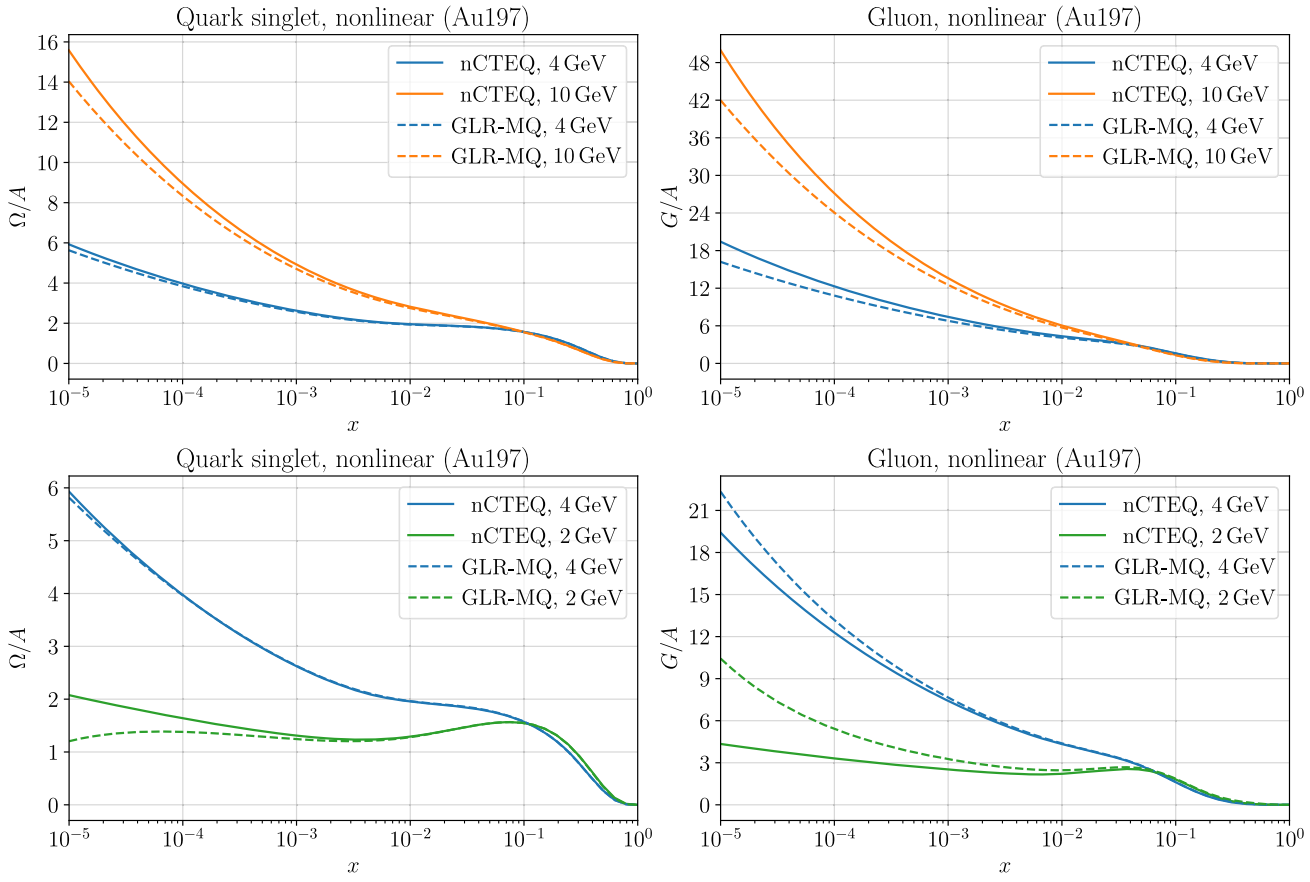

FIG. 2. Results of the nonlinear GLR-MQ evolution equations for nPDFs of the nucleus of Au-197. The quark singlet $\Omega(x, Q^2)$ and the gluon $G(x, Q^2)$ distributions per nucleon (dashed lines) are shown as a function of x after the upward evolution from $Q_0 = 2$ GeV to $Q = 4$ GeV and $Q = 10$ GeV (two upper panels) and after the downward evolution from $Q_0 = 10$ GeV to $Q = 4$ GeV and $Q = 2$ GeV (two lower panels) using the nCTEQ15 input. For comparison, the solid curves show the results of the nCTEQ parametrization at the corresponding values of Q.

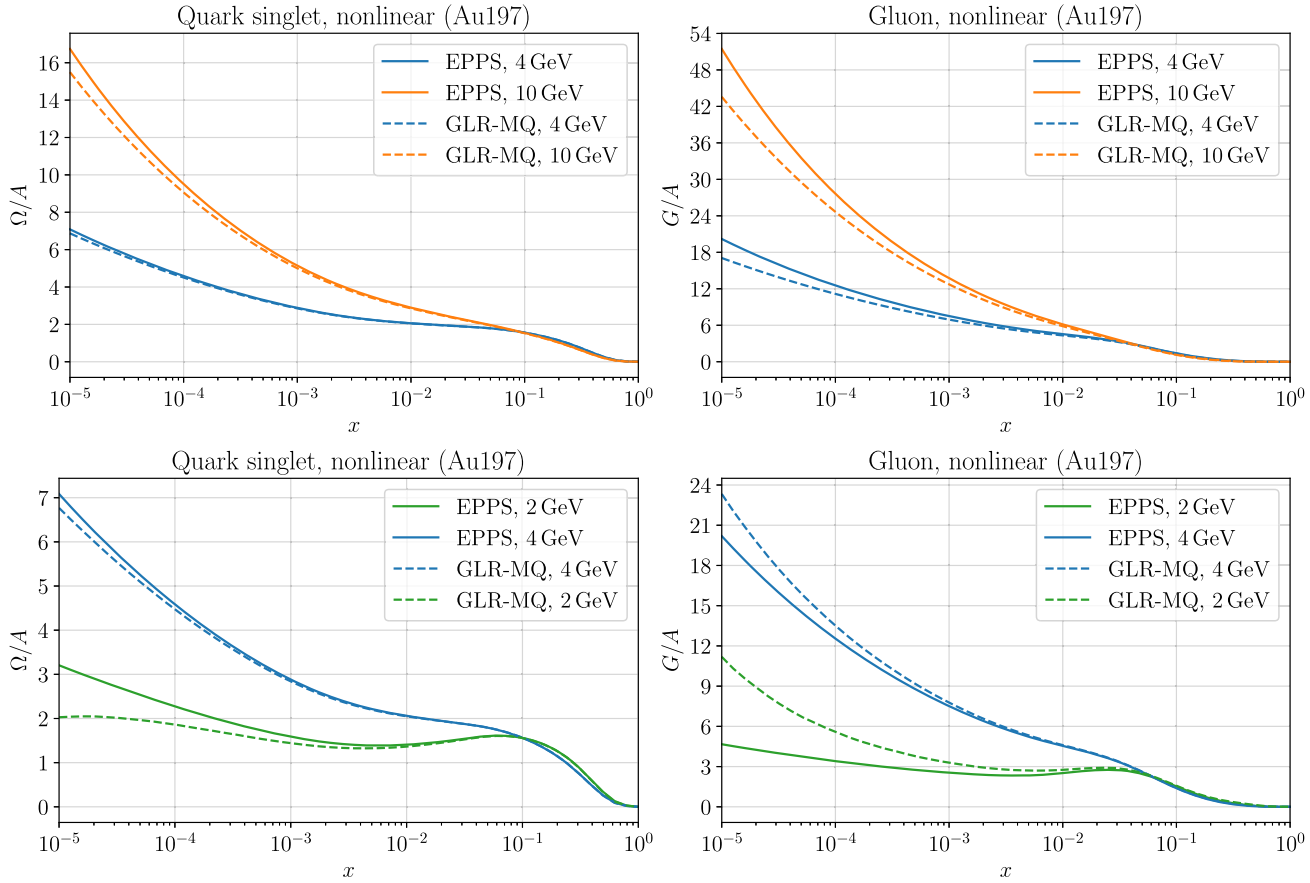

FIG. 3. The same as Fig. 2, but with the EPPS21 nPDFs.

of low-x gluons into high-x gluons slows down the growth of both gluon and quark singlet distributions for $x < 10^{-3}$. Since the gluon-quark splitting function $P_{FG}(x/z)$ is positive for $x \leq z \leq 1$, the lower gluon PDFs lead to a smaller rate of change $\Omega'(x, Q^2)$ and, consequently, to the observed decrease in $\Omega(x, Q^2)$. The absolute difference between the GLR-MQ and DGLAP evolved PDFs is generally smaller for the quark distribution. For instance, the values of $\Omega(x, Q^2)$ and $G(x, Q^2)$ at $Q = 10$ GeV and $x = 10^{-5}$ are reduced by 10% and 14%, respectively, compared to the corresponding nCTEQ15 PDFs.

The nonlinear terms in the GLR-MQ equations are suppressed as $1/Q^2$ and, hence, evolving downwards from a high value of Q_0 should in principle give a more accurate picture of the importance of the gluon recombination effect due to the evolution because the input is now insignificantly affected by gluon recombination. This is presented in the two lower panels of Fig. 2 showing by the dashed curves the results of the downward evolution from $Q_0 = 10$ GeV down to $Q = 4$ GeV and $Q = 2$ GeV. The relative deviation from the nCTEQ15 parametrization given by the solid curves is notably larger than for the upward evolution because the quark and gluon distributions are much smaller at low Q. For instance, at $Q = 2$ GeV and $x = 10^{-5}$, $\Omega(x, Q^2)$ is decreased by 43% compared to the nCTEQ15 PDFs, while $G(x, Q^2)$ is increased by 133%. At the same time, the absolute difference between the GLR-MQ and DGLAP evolved PDFs is similar for both evolution directions.

The gluon distribution after the downward evolution can be seen as a consequence of reversed gluon-gluon recombination, i.e., the migration of high-x gluons towards low x leading to the observed increase. As in the case of the upward evolution, the change in $G(x, Q^2)$ affects $\Omega(x, Q^2)$ mostly through the $P_{FG}(x/z)$ splitting function. The gluon-quark splitting in the case of the downward evolution corresponds to quark-antiquark pairs recombining into gluons, which explains the decrease in $\Omega(x, Q^2)$ observed in the lower left panel of Fig. 2.

To better understand and isolate the role of the gluon recombination effects in the evolution of quarks, we also solved the GLR-MQ equations without parton mixing by setting $P_{FG} = P_{GF} = 0$. We observed that this essentially stops the Q^2 evolution of the quark singlet distribution, which indicates that the combined effect of the quark-quark splitting and the gluon-quark recombination is very small

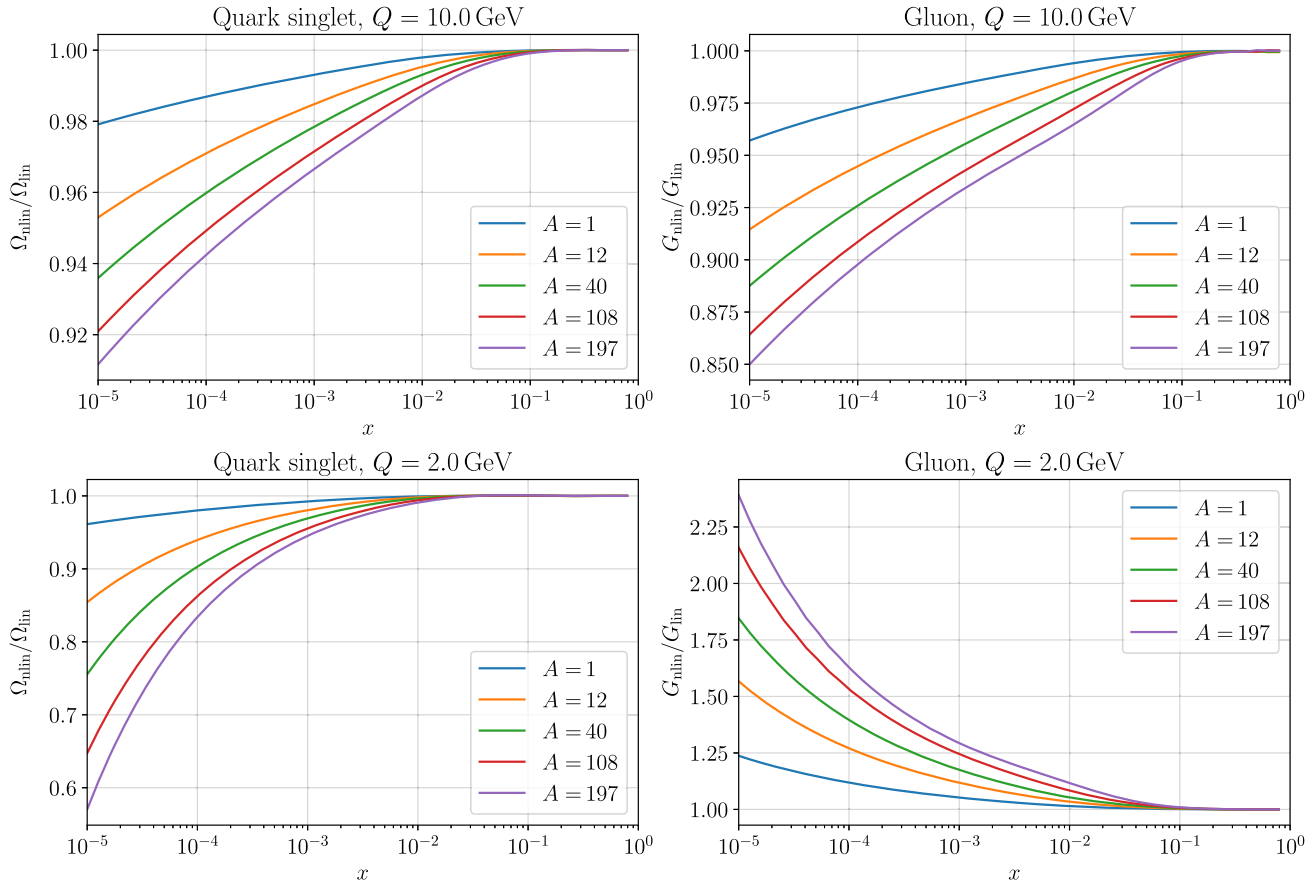

FIG. 4. The ratios of the quark singlet $\Omega_{\mathrm{nlin}}(x, Q^2)/\Omega_{\mathrm{lin}}(x, Q^2)$ and gluon $G_{\mathrm{nlin}}(x, Q^2)/G_{\mathrm{lin}}(x, Q^2)$ distributions after the GLR-MQ and DGLAP evolution, respectively, as a function of x for a wide range of nuclei including C-12, Ca-40, Ag-108, Au-197, and the free proton. The upper panels correspond to the upward evolution from $Q_0 = 2$ GeV to $Q = 10$ GeV; the lower panels are the results of the downward evolution from $Q_0 = 10$ GeV to $Q = 2$ GeV. As input, the nCTEQ15 nPDFs have been used.

compared to that of the neglected gluon-quark splitting. Consequently, the differences between the GLR-MQ and the DGLAP evolved quark PDFs can mainly be attributed to the $g - g$ recombination. This is consistent with the predictions made by Mueller and Qiu [8].

We also repeated our analysis using the EPPS21 nPDFs as input; the corresponding results are presented in Fig. 3. A comparison of these results to those in Fig. 2 shows that they are quantitatively very similar. Therefore, our conclusions on the trends and magnitudes of the nonlinear effects in the GLR-MQ equations very weakly depend on the choice of input nPDFs.

Figure 4 quantifies the size of the nonlinear corrections as a function of the mass number A. It presents the ratios of the quark singlet and gluon distributions after the GLR-MQ and DGLAP evolution denoted by $\Omega_{\mathrm{nlin}}(x, Q^2)/\Omega_{\mathrm{lin}}(x, Q^2)$ and $G_{\mathrm{nlin}}(x, Q^2)/G_{\mathrm{lin}}(x, Q^2)$, respectively, as a function of x for a wide range of nuclei including C-12, Ca-40, Ag-108, Au-197, and the free proton. As input, we used the nCTEQ15 nPDFs. The two upper panels correspond to the result of the upward evolution from $Q_0 = 2$ GeV to $Q = 10$ GeV; the two lower panels are the results of the downward evolution from $Q_0 = 10$ GeV to $Q = 2$ GeV. One can see from the figure that the nonlinear effects clearly become more important with increasing A. For example, at $x = 10^{-5}$, the upward evolution result for the proton gluon distribution is modified by about 4.5% and for the Au-197 distribution by about 15%. The difference between the GLR-MQ and DGLAP evolved PDFs grows steadily with a decrease of x; it is largest at the smallest values of x and disappears for $x \geq 0.1$. This behavior matches the approximate analytical solutions of the GLR-QM equations obtained by other groups [19–21].

As in the case of Fig. 2, we find that the nonlinear terms have a much bigger relative impact on the downward evolution for all considered nuclei and the proton. As explained previously, the nonlinear corrections suppress the quark singlet distribution and increase the gluon one. For very small x and heavy nuclei, the effect is $\mathcal{O}(30\text{–}40\%)$ for the quarks and $\mathcal{O}(100\text{–}140\%)$ for the gluons.

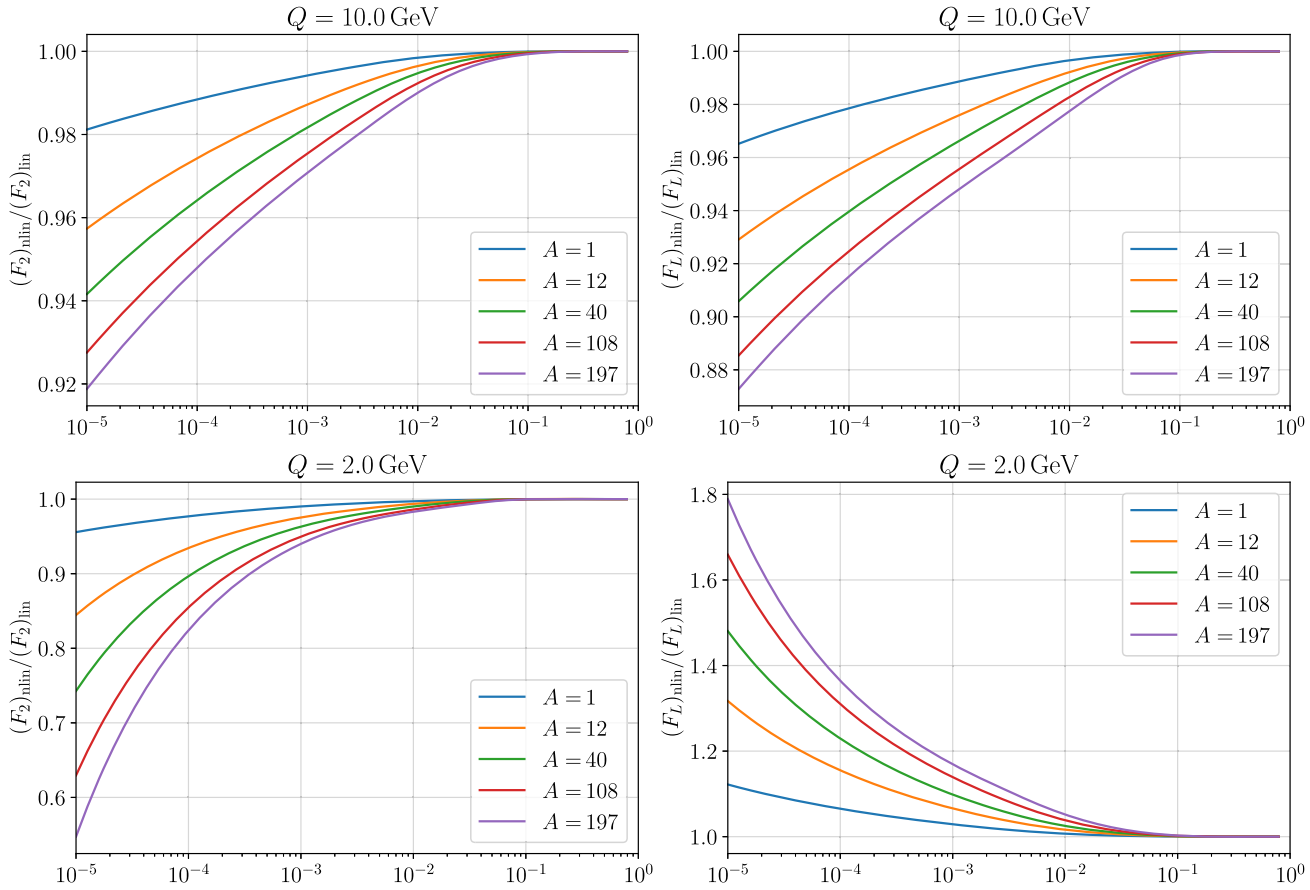

FIG. 5. The ratios of the $F_2^A(x, Q^2)$ (left panels) and $F_L^A(x, Q^2)$ (right panels) structure functions evaluated using the nuclear PDFs evolved according to the GLR-MQ and DGLAP evolution equations, respectively, as a function of x. As in Fig. 4, the upper panels correspond to the upward evolution from $Q_0 = 2$ GeV to $Q = 10$ GeV, and the lower panels are for the downward evolution from $Q_0 = 10$ GeV to $Q = 2$ GeV. As input, the nCTEQ15 nPDFs have been used.

Using the obtained nuclear PDFs, one can readily calculate the NLO nuclear structure function $F_2^A(x, Q^2)$,

$$F_2^A(x,Q^2) = N(x,Q^2) + \frac{\alpha_s(Q^2)}{2\pi}\int_x^1 \frac{dz}{z^2} x C_{2q}^{(1)}\left(\frac{x}{z}\right) N(z,Q^2) + \langle e^2\rangle \Omega(x,Q^2) + \langle e^2\rangle \frac{\alpha_s(Q^2)}{2\pi}\int_x^1 \frac{dz}{z^2} x C_{2q}^{(1)}\left(\frac{x}{z}\right)\Omega(z,Q^2) + \langle e^2\rangle \frac{\alpha_s(Q^2)}{2\pi}\int_x^1 \frac{dz}{z^2} x C_{2g}^{(1)}\left(\frac{x}{z}\right) G(z,Q^2), \tag{15}$$

and the longitudinal structure function $F_L^A(x, Q^2)$,

$$F_L^A(x,Q^2) = \frac{\alpha_s(Q^2)}{2\pi}\int_x^1 \frac{dz}{z^2} x C_{Lq}^{(1)}\left(\frac{x}{z}\right) N(z,Q^2) + \langle e^2\rangle \frac{\alpha_s(Q^2)}{2\pi}\int_x^1 \frac{dz}{z^2} x C_{Lq}^{(1)}\left(\frac{x}{z}\right)\Omega(z,Q^2) + \langle e^2\rangle \frac{\alpha_s(Q^2)}{2\pi}\int_x^1 \frac{dz}{z^2} x C_{Lg}^{(1)}\left(\frac{x}{z}\right) G(z,Q^2). \tag{16}$$

In Eqs. (15) and (16), $N(x, Q^2) = x\sum_{i=1}^{N_F} e_i^2 q_i^+(x, Q^2)$ and $q_i^+ = q_i(x, Q^2) + \bar{q}_i(x, Q^2) - 1/N_F \Sigma(x, Q^2)$ are nonsinglet quark distributions with N_F being the number of active flavors; $\langle e^2\rangle = (1/N_F)\sum_{i=1}^{N_F} e_i^2$; $C_{2q}^{(1)}$, $C_{Lq}^{(1)}$, $C_{2g}^{(1)}$, and $C_{Lg}^{(1)}$ are the standard quark and gluon coefficient functions, respectively. The convolution integrals in Eqs. (15) and (16) have exactly the same structure as those in the DGLAP evolution equations and, hence, the numerical method explained in Sec. II can be used to evaluate them.

Since the nonsinglet distribution $N(x, Q^2)$ is independent of $G(x, Q^2)$, we directly use the nCTEQ15 parametrization for it.

Figure 5 shows the ratios of the $F_2^A(x, Q^2)$ (left panels) and $F_L^A(x, Q^2)$ (right panels) structure functions evaluated using the nuclear PDFs, which were evolved according to the GLR-MQ and DGLAP evolution equations, respectively, employing the nCTEQ15 input. The ratios are denoted by $(F_2)_{\text{nlin}}/(F_2)_{\text{lin}}$ and $(F_L)_{\text{nlin}}/(F_L)_{\text{lin}}$ and are plotted as a function of x for C-12, Ca-40, Ag-108, Au-197, and the free proton. The trends of the A and x dependence mirror those of nPDFs shown in Fig. 4, where $F_2^A(x, Q^2)$ is dominated by $\Omega(x, Q^2)$ and $F_L^A(x, Q^2)$ by $G(x, Q^2)$. The nonlinear effects are again most important for heavy nuclei, and their impact is larger for $F_L^A(x, Q^2)$ than for $F_2^A(x, Q^2)$. Thus, it should be easier to observe them experimentally by measuring $F_L^A(x, Q^2)$. For instance, when evolving upward, the structure function $F_L(x, Q^2)$ for the proton is modified by about 3.5% at $x = 10^{-5}$, see the upper right panel. A similar-size effect can already be observed at $x = 4 \times 10^{-3}$ for Au-197.

Note that the momentum sum rule for nPDFs is slightly violated in the GLM-MQ approach since the gluon-gluon recombination leads to a suppression of the singlet quark and gluon nPDFs after the upward evolution and to a suppression of the singlet quark and an enhancement of the gluon nPDFs after the downward evolution. In particular, we find in the case of Au-197 that the total momentum sum rule is violated by approximately 5% after the upward evolution and by less than 3% after the downward evolution.

A generalization of this approach, which corrects this shortcoming and is valid in the whole x region, was suggested [9]. In our analysis, we focus only on the small x region and, hence, do not address the issue of the momentum sum rule, which affects the picture of nuclear modifications of nPDFs, including the valence quarks, in a broad range of x.

IV. CONCLUSIONS

In this paper, we numerically studied the GLR-MQ evolution equations for nPDFs to NLO accuracy and quantified the impact of gluon recombination at small x. Using the nCTEQ15 and EPPS21 nPDFs as input, we confirmed the importance of the nonlinear corrections for small $x \lesssim 10^{-3}$, whose magnitude increases with a decrease of x and an increase of the atomic number A. For instance, at $x = 10^{-5}$ and for heavy nuclei, after the upward evolution from $Q_0 = 2$ GeV to $Q = 10$ GeV, the quark singlet $\Omega(x, Q^2)$ and the gluon $G(x, Q^2)$ distributions become reduced compared to the results of the nCTEQ15 parametrization by 9–15%, respectively. The relative effect is much stronger for the downward evolution from $Q_0 = 10$ GeV to $Q = 2$ GeV, where we find that $\Omega(x, Q^2)$ is suppressed by 40%, while $G(x, Q^2)$ is enhanced by 140%. This is a consequence of the fact that the gluon-gluon recombination plays a much bigger role than the gluon-quark splitting.

The observed trend of the behavior of nPDFs affects the $F_2^A(x, Q^2)$ and $F_L^A(x, Q^2)$ nuclear structure functions. In particular, we find that after the downward evolution from high to low Q and for heavy nuclei and very small x, the $F_2^A(x, Q^2)$ structure function, which is dominated by $\Omega(x, Q^2)$, is reduced by 45%, while the $F_L^A(x, Q^2)$ longitudinal structure function, which is predominantly sensitive to $G(x, Q^2)$, is enhanced by 80%. Our analysis indicates that the nonlinear effects are most pronounced in $F_L^A(x, Q^2)$ and are already quite sizable at $x \sim 10^{-3}$ for heavy nuclei. Since the results employing the EPPS21 nPDFs are quantitatively similar, our predictions very weakly depend on the choice of input nPDFs.

ACKNOWLEDGMENTS

The work of V. G. is supported by the Academy of Finland (Project No. 330448), the Centre of Excellence in Quark Matter (Project No. 346326), the European Research Council project ERC-2018-ADG-835105 YoctoLHC, and also partially by a grant of Deutscher Akademischer Austauschdienst (DAAD). V. G. and J. R. would also like to thank Institut für Theoretische Physik, Westfälische Wilhelms-Universität Münster for hospitality. M. K. thanks the School of Physics at the University of New South Wales in Sydney, Australia for its hospitality and financial support through the Gordon Godfrey visitors program. The work of M. K. was also funded by the DFG through Grants No. KL 1266/9-1 and No. 10-1, the Research Training Group 2149 "Strong and Weak Interactions—from Hadrons to Dark Matter," and the Sonderforschungsbereich 1225 "Isoquant," Project-ID 273811115.

[1] R. Brock *et al.* (CTEQ Collaboration), Rev. Mod. Phys. **67**, 157 (1995).
[2] Y. L. Dokshitzer, Sov. Phys. JETP **46**, 641 (1977).
[3] V. N. Gribov and L. N. Lipatov, Sov. J. Nucl. Phys. **15**, 438 (1972).
[4] V. N. Gribov and L. N. Lipatov, Sov. J. Nucl. Phys. **15**, 675 (1972).
[5] G. Altarelli and G. Parisi, Nucl. Phys. **B126**, 298 (1977).
[6] Y. L. Dokshitzer, D. Diakonov, and S. I. Troian, Phys. Rep. **58**, 269 (1980).
[7] L. V. Gribov, E. M. Levin, and M. G. Ryskin, Phys. Rep. **100**, 1 (1983).
[8] A. H. Mueller and J. w. Qiu, Nucl. Phys. **B268**, 427 (1986).
[9] W. Zhu and J. h. Ruan, Nucl. Phys. **B559**, 378 (1999).
[10] Y. V. Kovchegov and E. Levin, *Cambridge Monograph Particle Physical Nuclear Physical Cosmology* (Cambridge University Press, Cambridge, England, 2012), Vol. 33, pp. 1–350, ISBN 978-0-521-11257-4, 978-1-139-55768-9.
[11] J. w. Qiu, Nucl. Phys. **B291**, 746 (1987).
[12] F. Gelis, E. Iancu, J. Jalilian-Marian, and R. Venugopalan, Annu. Rev. Nucl. Part. Sci. **60**, 463 (2010).
[13] J. Bartels, G. A. Schuler, and J. Blumlein, Z. Phys. C **50**, 91 (1991).
[14] K. J. Eskola, J. w. Qiu, and X. N. Wang, Phys. Rev. Lett. **72**, 36 (1994).
[15] E. Laenen and E. Levin, Nucl. Phys. **B451**, 207 (1995).
[16] K. Prytz, Eur. Phys. J. C **22**, 317 (2001).
[17] K. J. Eskola, H. Honkanen, V. J. Kolhinen, J. w. Qiu, and C. A. Salgado, Nucl. Phys. **B660**, 211 (2003).
[18] G. R. Boroun, Eur. Phys. J. A **42**, 251 (2009).
[19] G. R. Boroun and S. Zarrin, Eur. Phys. J. Plus **128**, 119 (2013).
[20] M. Lalung, P. Phukan, and J. K. Sarma, Nucl. Phys. **A984**, 29 (2019).
[21] M. Devee and J. K. Sarma, Nucl. Phys. **B885**, 571 (2014).
[22] H. Mäntysaari and B. Schenke, Phys. Rev. Lett. **117**, 052301 (2016).
[23] A. Accardi, J. L. Albacete, M. Anselmino, N. Armesto, E. C. Aschenauer, A. Bacchetta, D. Boer, W. K. Brooks, T. Burton, N. B. Chang *et al.*, Eur. Phys. J. A **52**, 268 (2016).
[24] J. L. Abelleira Fernandez *et al.* (LHeC Study Group), J. Phys. G **39**, 075001 (2012).
[25] O. Brüning and M. Klein (LHeC and PERLE Collaborations), J. Phys. G **46**, 123001 (2019).
[26] A. Abada *et al.* (FCC Collaboration), Eur. Phys. J. C **79**, 474 (2019).
[27] M. Botje, QCDNUM16: A fast QCD evolution program (1997), https://www.nikhef.nl/~h24/qcdnum/.
[28] K. Kovarik, A. Kusina, T. Jezo, D. B. Clark, C. Keppel, F. Lyonnet, J. G. Morfin, F. I. Olness, J. F. Owens, I. Schienbein *et al.*, Phys. Rev. D **93**, 085037 (2016).
[29] K. J. Eskola, P. Paakkinen, H. Paukkunen, and C. A. Salgado, Eur. Phys. J. C **82**, 413 (2022).
[30] W. Furmanski and R. Petronzio, Phys. Lett. **97B**, 437 (1980).
[31] S. Alekhin, O. Behnke, P. Belov, S. Borroni, M. Botje, D. Britzger, S. Camarda, A. M. Cooper-Sarkar, K. Daum, C. Diaconu *et al.*, Eur. Phys. J. C **75**, 304 (2015).
[32] H. Abdolmaleki *et al.* (xFitter Collaboration), arXiv:2206.12465.
[33] A. Buckley, J. Ferrando, S. Lloyd, K. Nordström, B. Page, M. Rüfenacht, M. Schönherr, and G. Watt, Eur. Phys. J. C **75**, 132 (2015).
[34] L. Frankfurt, V. Guzey, A. Stasto, and M. Strikman, Rep. Prog. Phys. **85**, 126301 (2022).